Electronic Supplementary Material (ESI) for Chemical Communications.

Supplementary Information

Interface-mediated formation of basic cobalt carbonate/polyethyleneimine composite microscrolls by strain-induced self-rolling

Viktoria Gruen,[a] Nicolas Helfricht,[b] Sabine Rosenfeldt[cd] and Anna S. Schenk[ad]*

[a]*Physical Chemistry – Colloidal Systems, University of Bayreuth, 95440 Bayreuth, Germany*

[b]*Physical Chemistry II, University of Bayreuth, 95440 Bayreuth, Germany*

[c]*Physical Chemistry I, University of Bayreuth, 95440 Bayreuth, Germany*

[d]*Bavarian Polymer Institute, University of Bayreuth, 95440 Bayreuth, Germany*

*E-mail: anna.schenk@uni-bayreuth.de

Contents

1. Experimental Details

1.1. Chemicals and Materials

Cobalt(II) chloride hexahydrate (≥ 99%, p.a.), ammonium carbonate, fluorescein isothiocyanate isomer I, and dimethylsulfoxid were purchased from Sigma Aldrich. Polyethyleneimine (PEI, branched, Mw~10,000 g/mol) was obtained from Alfa Aesar. All chemicals were used directly as obtained from the supplier and aqueous solutions were prepared with deionized water (resistivity 18.2 MΩcm, Milli-Q Advantage A10, Merck)

1.2. Preparation of Basic Cobalt Carbonate Curls and Transformation into Co_3O_4. A gas diffusion technique based on the slow decomposition of ammonium carbonate was applied for the interface-directed precipitation of basic cobalt carbonate. For that purpose, aqueous solutions of cobalt chloride hexahydrate ($[Co^{2+}]$ = 25 mM or 100 mM) were prepared in the absence ([PEI] = 0 g/L) and presence ([PEI] = 0.05 g/L, 0.5 g/L, 1 g/L, 2 g/L, 5 g/L and 10 g/L) of PEI (*cf*. scheme 1) as a structure-directing additive. A total volume of 5 mL of each reaction mixture was pipetted into a 10 mL glass vial covered with Parafilm, into which three holes were punched with a fine needle. The reaction vials were then transferred into a sealed desiccator (DN 200) together with two glass vials, each containing 5 g $(NH_4)_2CO_3$. The $CoCl_2$/PEI reactant solutions were exposed to the CO_2 and NH_3 vapour formed upon decomposition of the solid for 24 h to induce basic cobalt carbonate precipitation. Subsequently the film-like material deposited at the air/solution interface was skimmed off with a spoon and carefully transferred onto pure water to rinse off any residual impurities. After removal of the water layer with filter paper, the samples were dried at room temperature. A minimum of 5 replicates were performed for each mineralization experiment. While the general tendency towards the formation of curling structures was highly reproducible across the batches, the deposited spirals varied in size and number of twists. Selected specimens with spiral morphology were converted into Co_3O_4 by calcination at 400°C for 24 hours.

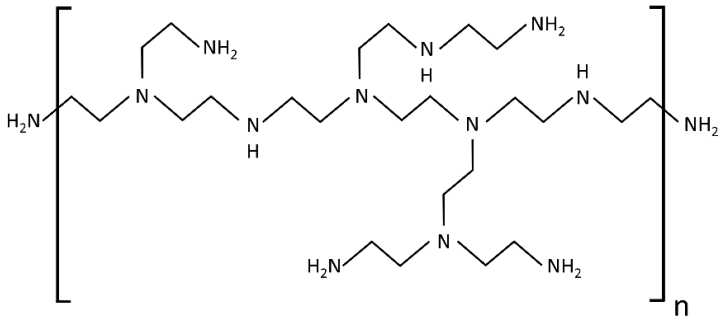

Scheme 1. Chemical structure of branched PEI comprising primary, secondary and tertiary amine groups.

1.3. Structural and Compositional Characterization.

The structure and composition of cobalt hydroxide carbonate precipitates obtained in the absence and presence of PEI as well as calcined samples were characterised using a wide range of analytical methods.

Digital Light Microscopy. General morphologies of film fragments and spirals were imaged by digital light microscopy using either a VHX-950F instrument equipped with a VH-Z250R objective or a Leica DVM6 M microscope with PLANAPO F0V 12.55 objective.

Scanning Electron Microscopy (SEM) and Energy-Dispersive Spectroscopy (EDS). Morphologies and detailed structures of the obtained basic cobalt carbonate film fragments were examined using a Zeiss LEO 1530 VP Gemini equipped with a Schottky-field-emission cathode and secondary electron as well as backscattered electron detectors. The elemental composition of polymer/mineral spirals was studied by EDS with an UltraDry SDD Noran system (Thermo Fisher Scientific). The instrument was operated at an acceleration voltage of 3 kV for SEM imaging and 20 kV for EDS analysis.

Prior to imaging, small film fragments were mounted on a standard sample holder using conductive adhesion graphite-pads (Plano, Wetzlar, Germany). For cross-sectional views, individual spirals were manually positioned with boar bristles and fixed with all-purpose glue. The samples were then either sputter-coated with platinum (1.3 - 2 nm thickness) using an HR208 sputter coater and an MTM-20 thickness controller (Cressington Scientific Instruments, Watford, United Kingdom) or vapour-coated with carbon using a Leica EM ACE600 system.

Attenuated Total Reflectance Fourier-Transform Infrared Spectroscopy (ATR-FTIR). FTIR spectra of powdered samples were recorded with a Bruker Tensor 27 instrument (Ettlingen, Germany) with Specac golden gate single reflection ATR. An atmospheric compensation algorithm was applied in the OPUS 8.0 software in order to correct for non-specific fluctuations due to CO_2 and water vapour during the measurement.

UV-Vis Spectroscopy. UV-Vis spectra of solutions containing 25 mM $CoCl_2$ and varying PEI concentrations ([PEI] = 0 g/L, 0.025 g/L, 0.05 g/L, 0.25 g/L, 0.5 g/L, 0.625 g/L, 0.875 g/L, 1 g/L, 1.25 g/L, 1.5 g/L or 1.75 g/L) were recorded with an Agilent UV-Vis spectrophotometer 8453 before (t = 0h) and after (t = 24 h) exposure to ammonium carbonate vapour.

Thermogravimetric Analysis (TGA) and High Temperature Differential Scanning Calorimetry (HDSC). The thermal stability and gradual decomposition of the interface-derived materials were analysed by TGA and HDSC performed with a Linseis STA PT 1600 instrument. Thermograms were recorded in a temperature

range between 30°C and 1000°C by heating 10-20 mg of the sample in a platinum crucible under air atmosphere at a heating rate of 10°C/min. Analysis was performed using the Linseis Platinium TA software.

Confocal Laser Scanning Microscopy (CLSM). For visualization by CLSM, PEI was fluorescently labeled with flourescein Isomer I. For that purpose, 2.5 g PEI (Mw~10.000 g/mol) were dissolved in 20 mL water and separately, 6.4 mg of the fluorescent dye (fluorescein isothiocyanate isomer I) were dissolved in 2 mL dimethylsulfoxid. The fluorophore solution was then added to the aqueous PEI solution and the mixture was subsequently stirred at room temperature for 24 hours followed by dialysis (ZelluTrans T1, 3.5kDa, Scienova) against water for 3 days. The solution was protected from illumination by light during the entire process. After functionalization, the flourescein-labeled polymer was used as a soluble additive in interface mediated mineralization (*cf.* chapter 1.2).

CLSM imaging was performed using a TCS SP8 instrument (Leica GmbH, Germany) equipped with a laser exhibiting an excitation wavelength of 488 nm. The absorption band of flourescein is observed at 492 nm and the emission was detected in the range between 500 nm and 555 nm (green) using a sensitive hybrid detector (HyD3). The images were acquired at a scan speed of 12 kHz using a frame average of 40. A resolution of 512 x 512 pixels results in a voxel-size of 0.455 µm in x- & y-direction. A z-stack of 120 µm was performed in 600 steps, which results in a voxel-size of 0.208 µm in z-direction. Associated bright field microscopy images were recorded by means of a photomultiplier. In order to image the curls prepared with unmodified PEI for comparison, a frame average of 128 frames was applied to increase the signal to noise ratio due to the very low fluorescent intensity observed.

Synchrotron Small-Angle X-Ray Scattering and Powder X-Ray Diffraction (SAXS and PXRD). An individual curl of interface-derived basic cobalt carbonate ([Ca^{2+}] = 25 mM, [PEI] = 0.5 g/L) before calcination and a powdered sample of such microscrolls after calcination at 400°C for 24 h were investigated by a combination of small-angle X-ray scattering (SAXS) and wide-angle x-ray scattering (WAXS). These experiments were performed at the MiNaXS/P03 beamline of the storage ring PETRA III at DESY, Hamburg at an energy of 13 keV (λ = 0.953 Å) with a beam size of 30 µm x 12 µm. The beam direction was perpendicular to the film surface in case of the individual spiral. Powdered samples were measured in glass capillaries. The obtained 2D data sets were recorded with Pilatus detectors (1M for SAXS and 300k for WAXS). Since all 2D scattering patterns appeared isotropic, the data were radially averaged. From these resulting scattering intensities, I(q) ($q = \frac{4\pi}{\lambda}\sin\left(\frac{\theta}{2}\right)$, λ wavelength, θ scattering angle), the signals of an empty capillary (for powdered samples) or air (for individual, free-standing curl) were subtracted as background.

2. Supplementary Figures and Analyses

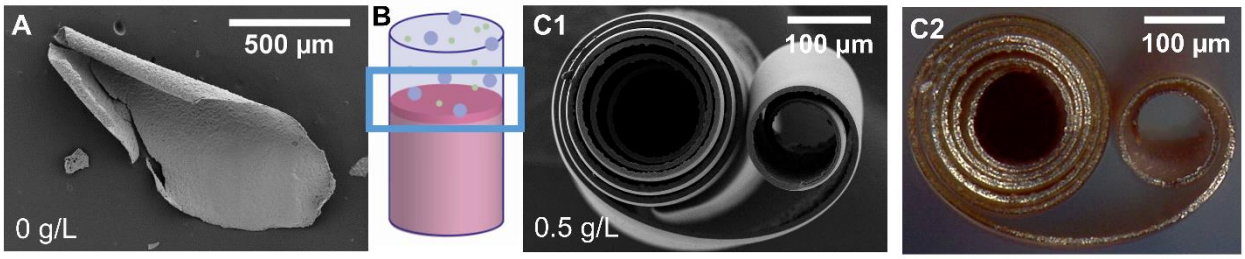

Figure S1. Morphologies of basic cobalt carbonate deposited at the air/solution interface in the absence and presence of polyethyleneimine (PEI, a). Precipitation of basic cobalt carbonate is induced by exposing $CoCl_2$ solutions ($[Co^{2+}]$ = 25 mM) to ammonium carbonate vapor in a sealed desiccator. The interface precipitate was separated from the solution after 24 hours. Drying at room temperature induces fragmentation of the solid sheets. (A) Scanning electron micrograph (SEM) of a representative film fragment deposited in the absence of PEI showing only a minor degree of wrinkling. In polymer-mediated mineralization ([PEI] = 0.5 g/L), the interfacial two-dimensional sheets (schematically illustrated as a dark pink layer in B; blue box marks the air/solution interface enriched in polymer) undergo pronounced self-rolling into spiral patterns with up to six narrow turns. SEM (C1) and digital light microscopy (C2) of the spiraling structure obtained in the presence of the polybase are shown.

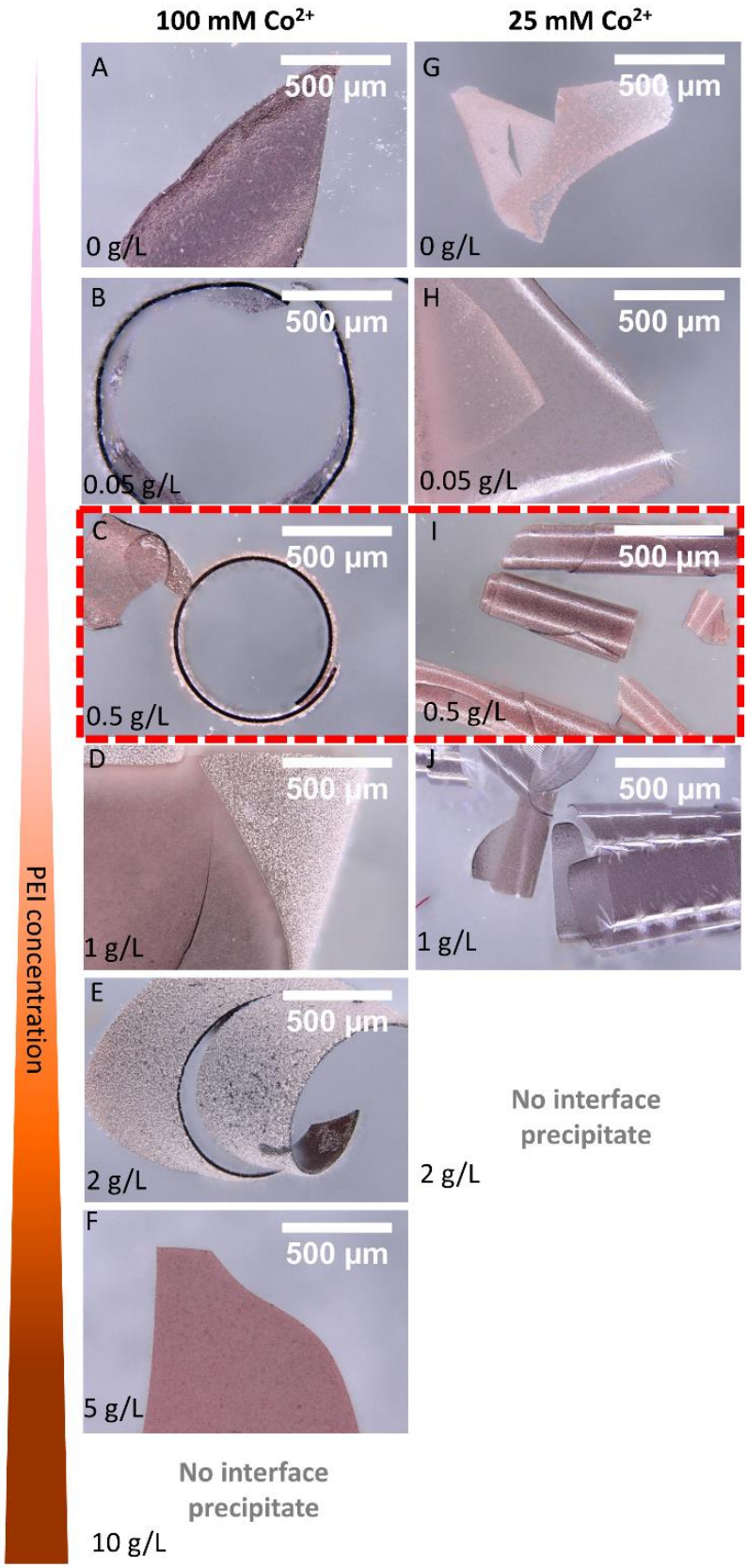
100 mM Co2+
25 mM Co2+
A
500 µm
0 g/L
G
500 µm
0 g/L
B
500 µm
0.05 g/L
H
500 µm
0.05 g/L
C
500 µm
0.5 g/L
I
500 µm
0.5 g/L
D
500 µm
1 g/L
J
500 µm
1 g/L
E
500 µm
2 g/L
No interface precipitate
2 g/L
F
500 µm
5 g/L
No interface precipitate
10 g/L
PEI concentration

Figure S2. Digital light microscopy of basic cobalt carbonate sheets obtained at different Co^{2+} and PEI concentrations. For both, $[Co^{2+}]$ = 100 mM (A-F) and $[Co^{2+}]$ = 25 mM (G-J) and, the tendency for spiraling increases with PEI content until a PEI concentration of [PEI] = 0.5 g/L is reached (corresponding to ratios [amine]/$[Co^{2+}]$ = 0.45 for 25 mM Co^{2+} and [amine]/$[Co^{2+}]$ = 0.11 for 100 mM Co^{2+}, respectively). At higher polymer concentrations, the number of twists adopted by the film fragments starts to decrease again and interface-mediated mineralization becomes entirely suppressed when an [amine]/$[Co^{2+}]$ ratio of ≈1.5 is exceeded.

Due to their lower thickness, and thus higher aspect ratio, film fragments obtained at $[Co^{2+}]$ = 25 mM (G-J) generally showed a higher tendency towards self-rolling than the ones obtained at a higher $CoCl_2$ concentration ($[Co^{2+}]$ = 100 mM). Based on these observations, the reaction conditions framed in red were identified as most favorable and used for further experiments.

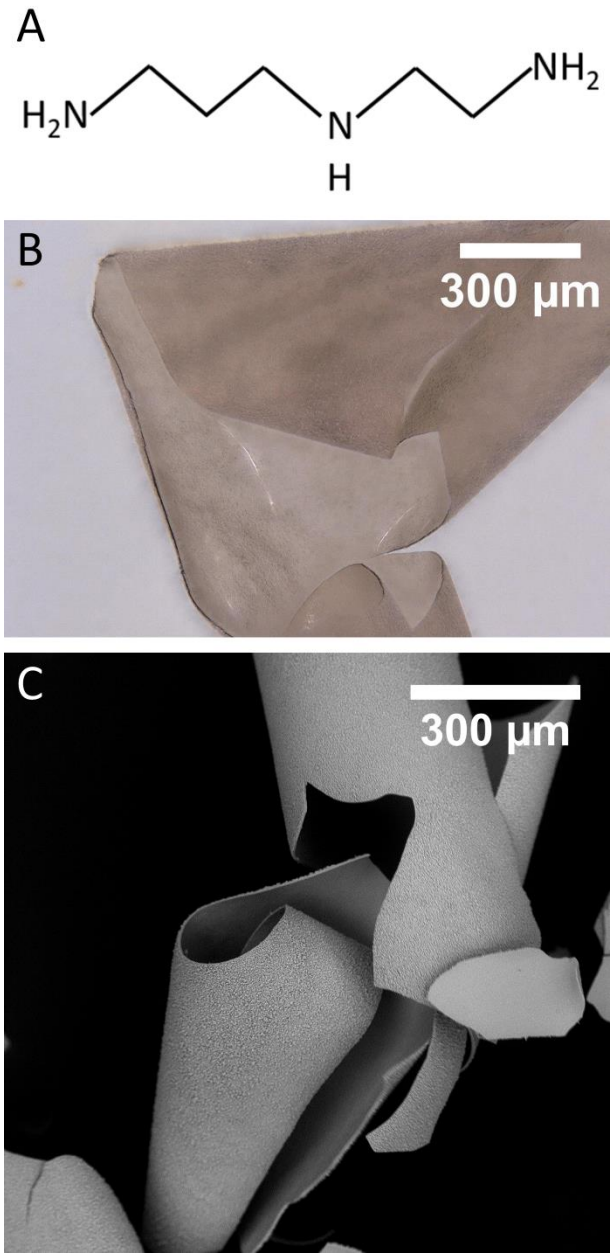

Figure S3. Basic cobalt carbonate sheets precipitated at the air/solution interface in the presence of the amine-functionalized small molecule N-(2-Aminoethyl)-1,3-propanediamine (A, [additive] = 0.5 g/L, $[Co^{2+}]$ = 25 mM) were examined by digital light microscopy (B) and SEM (C). The film fragments showed a slight tendency for curling, but exhibited a lower symmetry and a reduced number of twists than observed in polymer-mediated samples at the same mass concentration of additives and Co^{2+} ions.

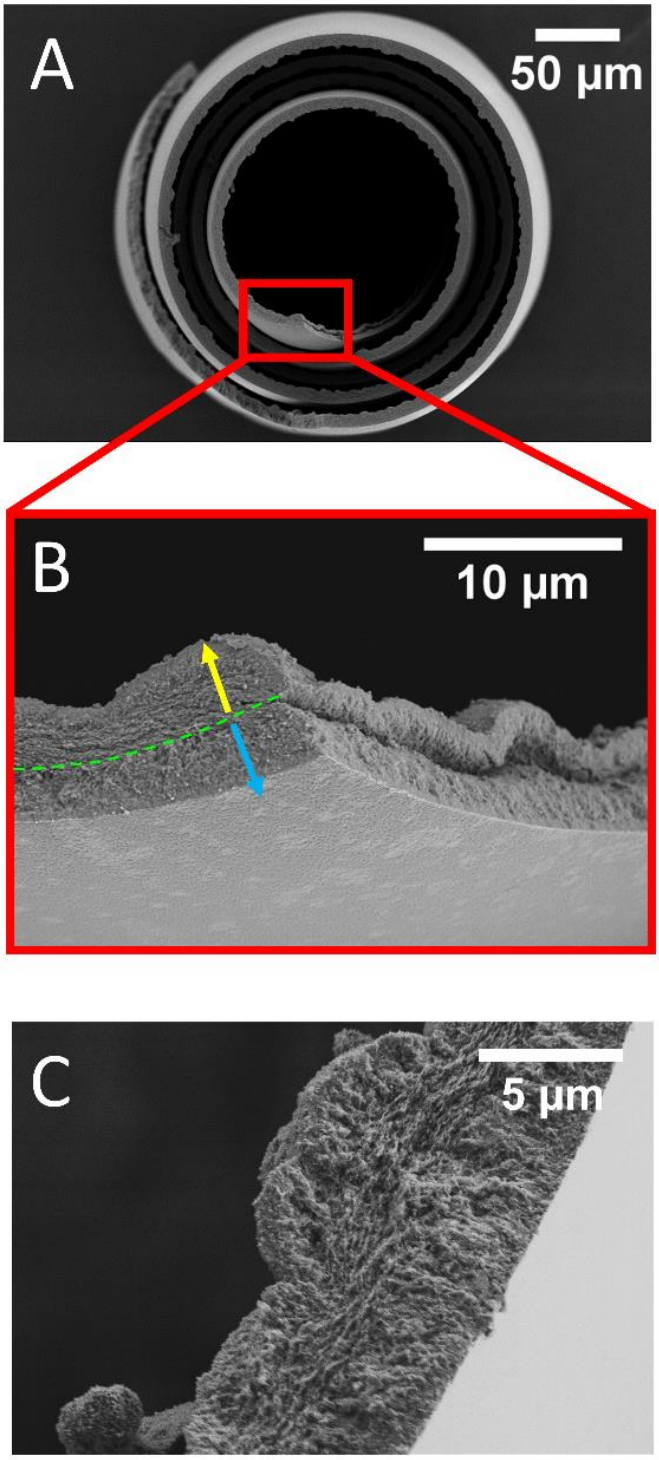

Figure S4. Scanning electron micrographs showing the cross-section of a representative curled mineral sheet deposited in the presence of PEI ([PEI] = 0.5 g/L). An overview image (A) as well as detailed views of the micro- (B) and mesostructure (C) are shown. The basic cobalt carbonate film fragment exhibits a thickness in the micrometer regime (A) and a conspicuous nanoscale granularity (B, C). Yellow and blue arrows in (B) indicate two (partially delaminated) layers of the mineral film presumably originating from

interfacially nucleated mineral formation along opposing growth directions (delineation of growth regimes highlighted by green, dotted line) pointing towards the vapor (yellow arrow) and the solution phase (blue arrow). The absence of larger micro-cracks on the outer surface of the spirals points to a strong capacity of the nano-granular amorphous basic cobalt carbonate to accommodate the strain built up during the curling deformation. Excess strain due to volume shrinkage upon drying appears to be preferentially released by fracture/delamination perpendicular to the surface normal direction (B).

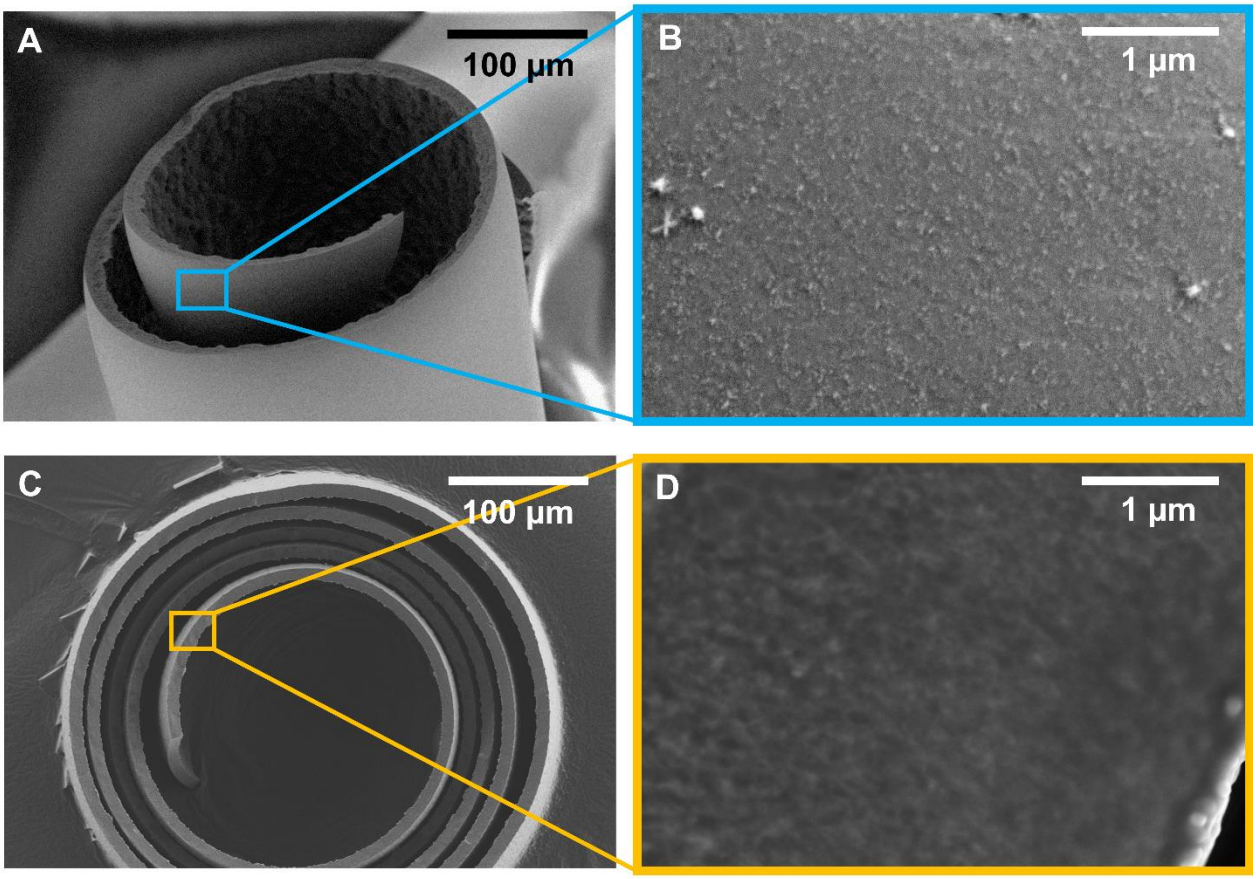

Figure S5. Scanning electron micrographs obtained from the surface of representative basic cobalt carbonate spirals comparing side view (A, B) and top view (C, D). While the outer surface appears remarkably smooth (A, B) and no obvious micro-cracks are seen, the cross sectional view reveals a fine-granular structure throughout the interface-grown mineral film (C, D).

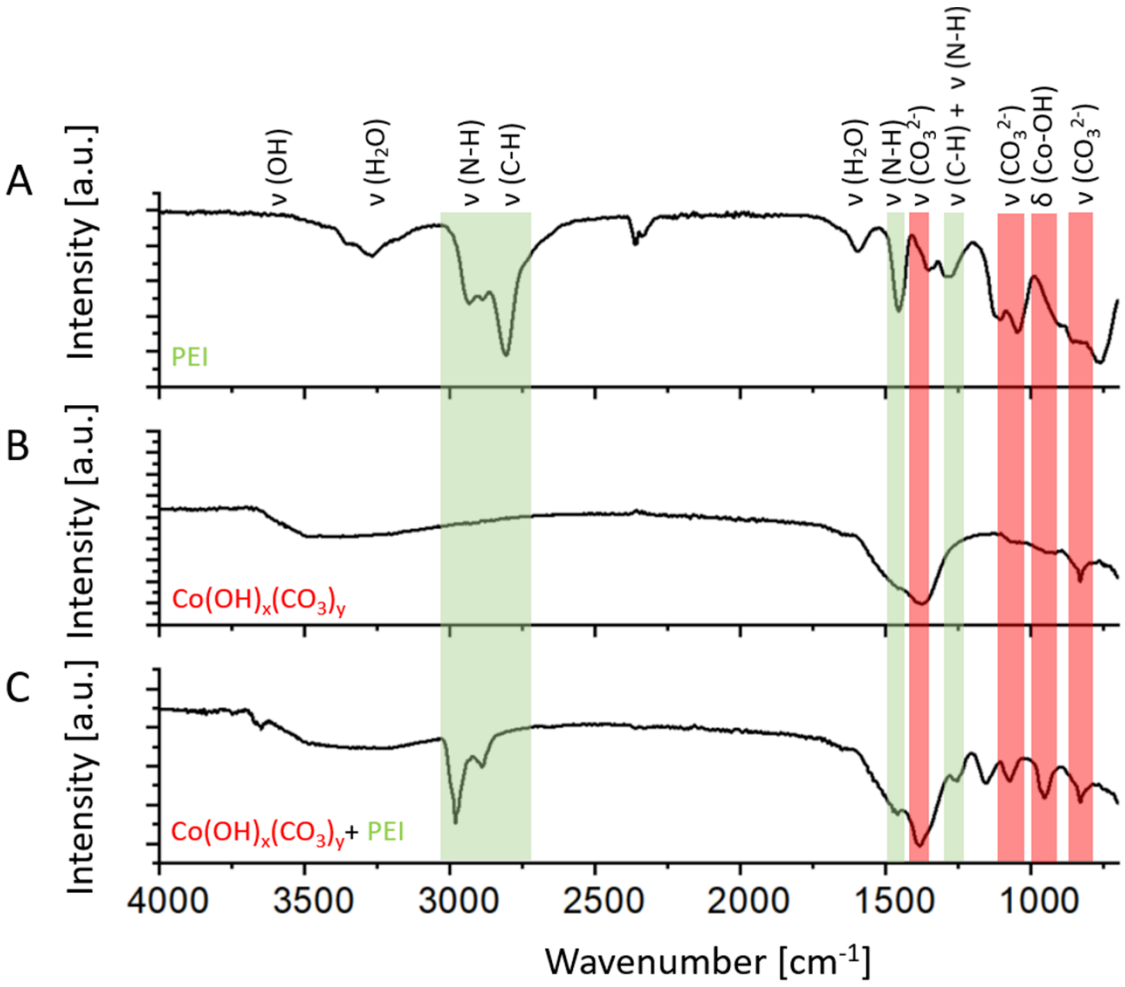

Figure S6. Fourier-transform infrared (FT-IR) spectra of pure PEI polymer (A) as well as interface-derived basic cobalt carbonate deposits obtained in the absence (B) and in the presence (C) of PEI ([PEI] = 0.5 g/L) are shown. Red bars highlight signals attributable to the basic cobalt carbonate mineral phase and green bars mark vibration bands associated with PEI. Specifically, signals centered at 1254 cm^{-1}, 1458 cm^{-1}, 2885 cm^{-1} and 2980 cm^{-1} correspond to characteristic vibrations of C-H and N-H bonds originating from PEI macromolecules.[1, 2] The presence of carbonate ions associated with the mineral phase is evidenced by vibration bands at 1072 cm^{-1} ($\nu_1(CO_3^{2-})$, presumably IR-active due to symmetry reduction and 1381 cm^{-1} ($\nu_3(CO_3^{2-})$).[3] In addition, the signal detected at 829 cm^{-1} can be assigned to the symmetric bending mode of carbonate ions. The δ(Co-OH) bending mode characteristic of basic cobalt carbonate is observed at 955 cm^{-1}, while the band detected at 1155 cm^{-1} corresponds to an asymmetric bridge oxygen stretching vibration representative of a cobalt hydroxide-based material.[4, 5] Broad signals observed at frequencies in the range between 2700 cm^{-1} and 3600 cm^{-1} in combination with the band at 1647 cm^{-1} are characteristic of intra-structural or surface-adsorbed water molecules. The sharper band at 3647 cm^{-1} observed in the composite material can be assigned to the stretching vibration of strongly bound hydroxyl molecules.

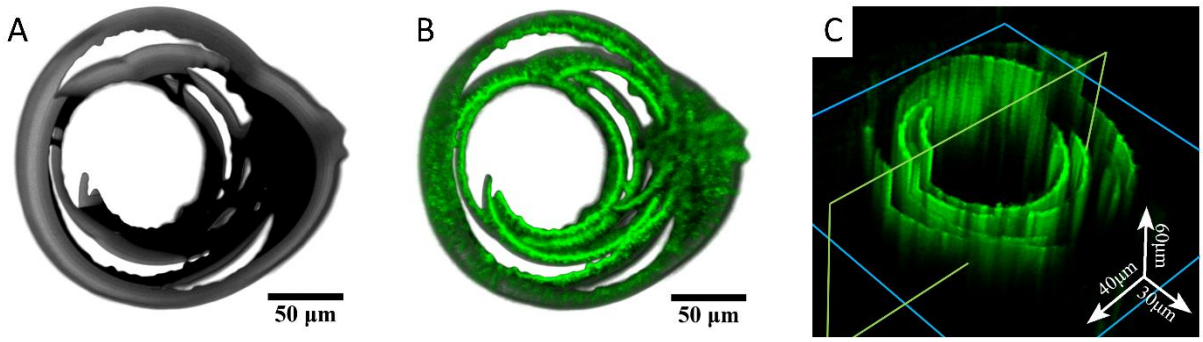

Figure S7. Visualization of the incorporation of fluorescently labeled PEI into a representative basic cobalt carbonate curl by confocal laser scanning microscopy (CLSM). The bright field image (A) demonstrates that the spiral morphology of interface-precipitated basic cobalt carbonate is preserved in the presence of fluorescein-labeled polymer ([PEI] = 0.5 g/L). A significant fluorescence signal indicating the presence of PEI associated with the mineral phase is seen in a combined bright field fluorescence image (B). A cross-sectional cut through a 3-dimensional reconstruction of the structure is shown in (C), where the pronounced fluorescence signal reveals incorporation of polymer inside the inorganic sheet.

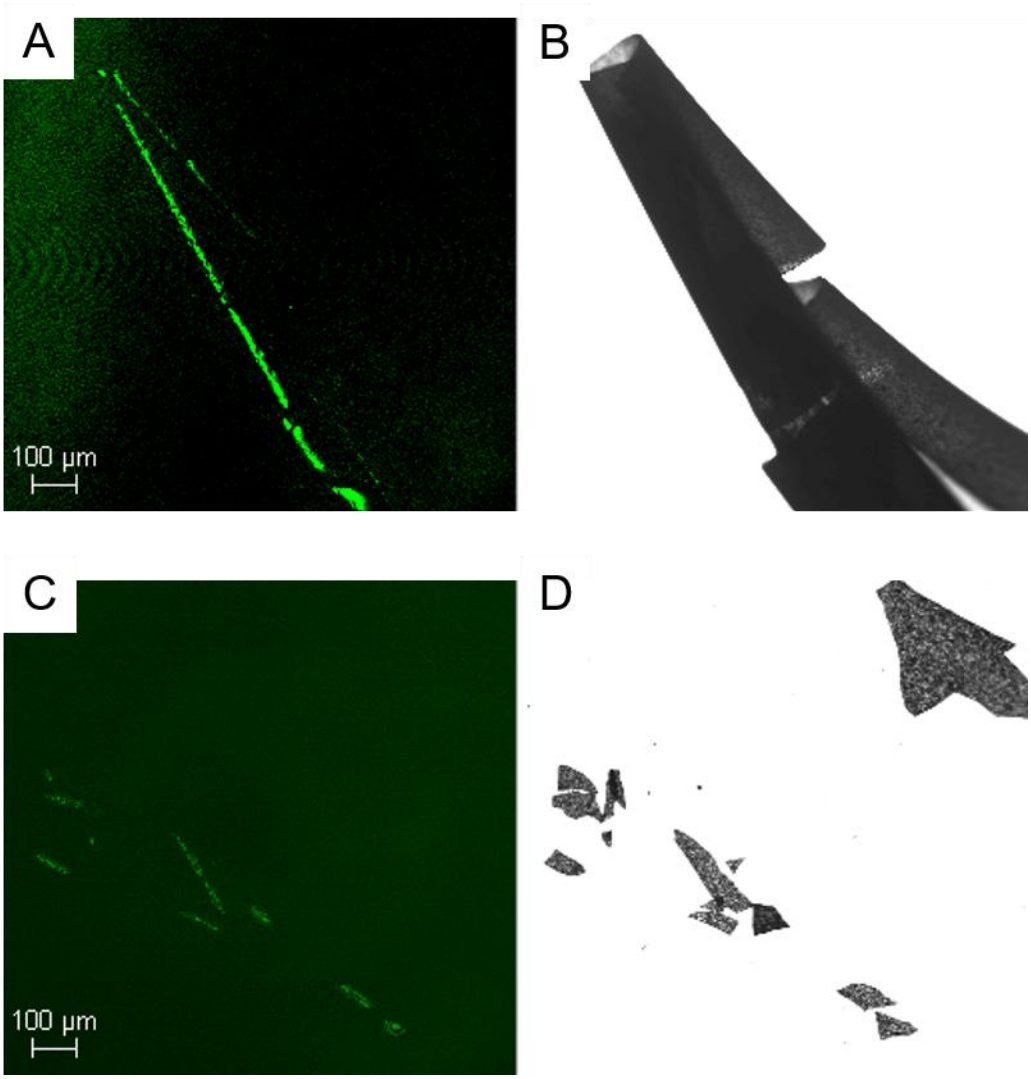

Figure S8. CLSM imaging of basic cobalt carbonate spirals as prepared with bare PEI ([PEI] = 0.5 g/L), i.e. in the absence of a fluorescent dye. Flourescence imaging of intact spirals (A) and two-dimensional fracture pieces (C) are shown together with the corresponding transmission light microscopy images (B and D). These images demonstrate that despite the substantially less intense signal compared to fluorescein-labeled PEI, the polybase itself can be detected within (or associated with) the mineral sheets, thus supporting the hypothesis of a composite nature.

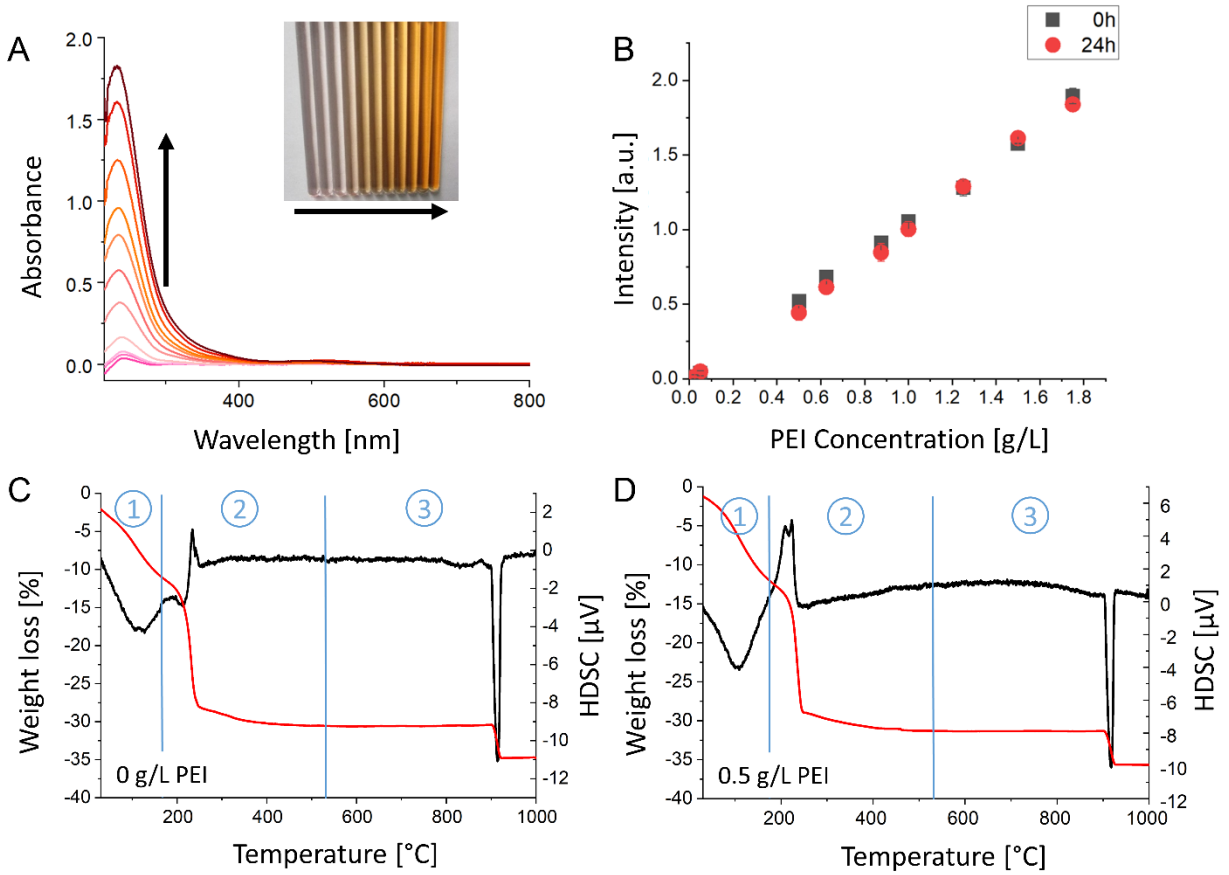

Figure S9. Composition of reactant solutions and mineralized products. (A) UV-Vis measurements of 25 mM $CoCl_2$ solutions in the presence of different amounts of PEI ([PEI] = 0 g/L, 0.025 g/L, 0.05 g/L, 0.25 g/L, 0.5 g/L, 0.625 g/L, 0.875 g/L, 1 g/L, 1.25 g/L, 1.5 g/L and 1.75 g/L, bottom to top). All PEI-containing solutions showed a characteristic absorption band at λ = 232 nm, which is attributed to the formation of Co(II)-PEI complexes,[6, 7] as well as a minor Co(II)-related signal at ~520 nm. The gradual intensity increase of this signal at 232 nm with increasing polymer concentration is accompanied by a visible color change of the solution from light pink to brown (Inset: photograph of Co^{2+}/PEI solutions, arrow indicates increasing PEI concentration). (B) The maximum intensities obtained at different PEI concentrations before (0 h, black squares) and after (24 h, red circles) exposure to ammonium carbonate vapor are plotted. Comparison of these data points does not indicate any substantial decay in PEI concentration upon induction of basic cobalt carbonate precipitation. (C, D) Thermogravimetric analysis (TGA, red line) and high temperature differential scanning calorimetry (HDSC, black line) measurements of mineral deposits obtained in the absence (C) and presence (D) of PEI. In both systems, a first weight loss event is observed in the temperature range between 30°C and ca. 175°C, which can be assigned to the evaporation of surface-bound and intra-structural water (region 1). Quantitatively, this water-related weight loss does not differ

between atmospherically dried basic cobalt carbonate films prepared in the absence or presence of the polybase. Hence, the addition of PEI does not significantly increase the amount of strongly bound intra-structural water. The major weight loss in region 2 is attributed to the release of CO_2 and H_2O associated with the conversion of basic cobalt carbonate to Co_3O_4 accompanied by the decomposition of PEI (literature reported decomposition temperatures in the range between 200°C and 400°C)[8]. The mass reduction (based on dry weight) accounts for 18.80 % in the case of the polymer-free system and 18.55 % for the mineral deposited in the presence of PEI. Hence, TGA cannot provide proof for the incorporation of a major amount of PEI within the polymer-mediated curls. Only the split HDSC signal may represent an indicator for incorporated organics. The final endothermal event observed in region 3 reflects the transformation from Co_3O_4 to CoO.

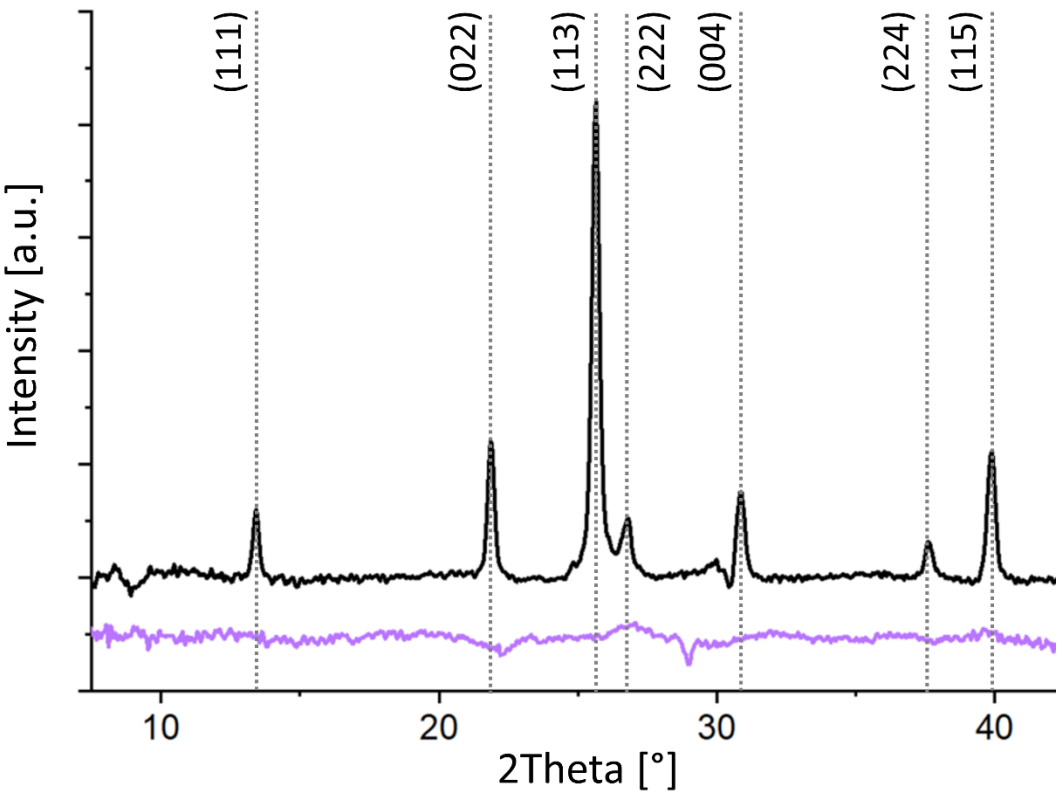

Figure S10. The powder X-ray diffractogram (PXRD) of curly basic cobalt carbonate ([Co^{2+}] = 25 mM, [PEI] = 0.5 g/L, violet curve) does not show any indication of crystallinity, while the diffraction pattern of the calcination product obtained after 24 h at 400°C (black curve) exhibits distinct diffraction peaks attributable to spinel-type cobalt(II/III) oxide (Co_3O_4, Reference code: PDF 96-153-8532[9])

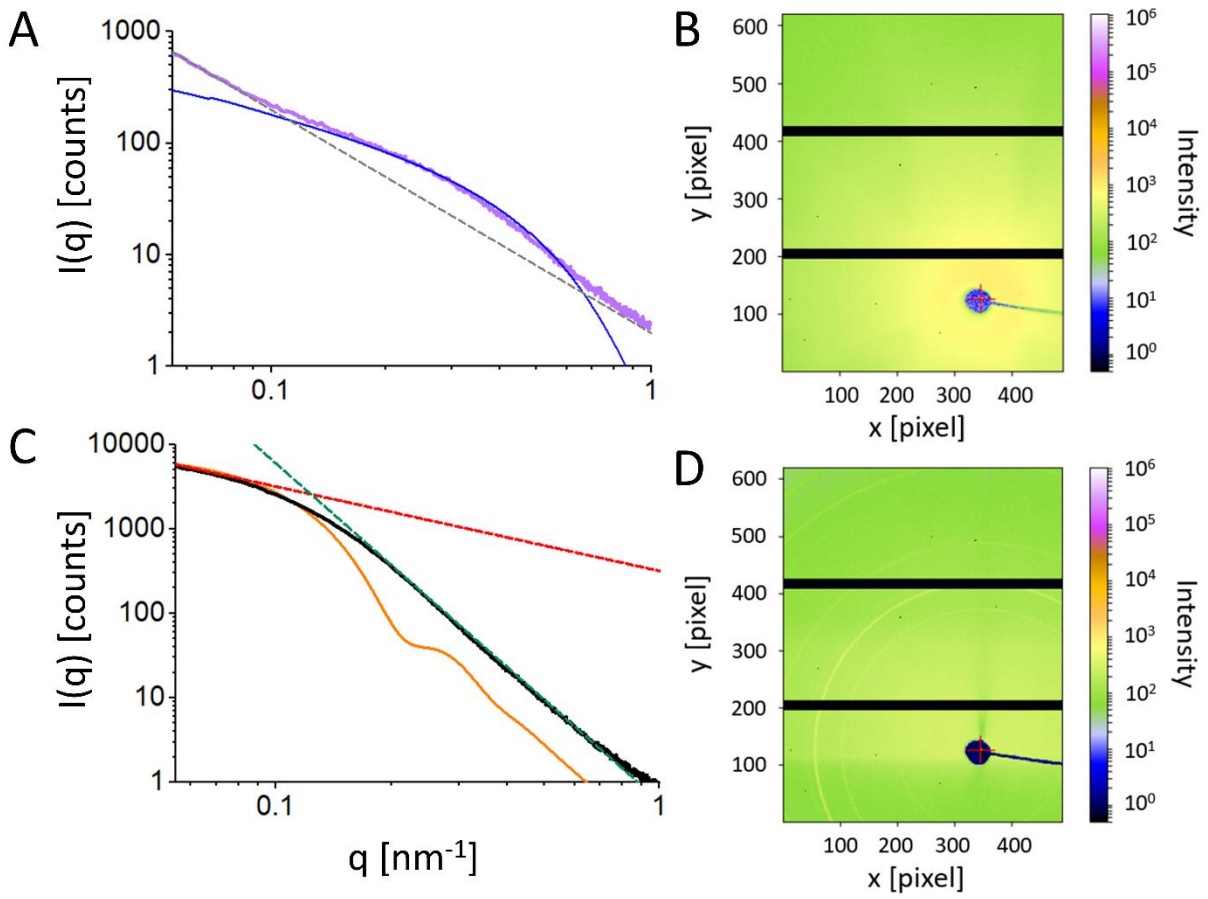

Figure S11. Small-angle X-ray scattering (SAXS) signals of (A, C) / WAXS (B, D) of an individual basic cobalt carbonate curl ([Co^{2+}] = 25 mM, [PEI] =0.5 g/L) before calcination (A, B; violet line) and a powdered sample of such polymer/mineral spirals after calcination at 400°C for 24 h (C, D; black line). For comparison, typical scaling laws are shown as dashed lines, in (A) q^{-2} (grey), and in (C) q^{-1} (red) and q^{-4} (green). The solid lines represent theoretical intensities of (A) circular cylinders (blue, radius R=3.5 nm (20% Gaussian distribution), length L=70 nm (15% Gaussian distribution)) or (C) homogeneous spheres (yellow, R=20 nm (15% Gaussian distribution).

Surface-sensitive SEM imaging (Figs. S4 and S5) points towards a sub-structuring of the mineral/PEI composite curls on the nanometer scale. To substantiate these results, X-ray scattering was performed as a volume-averaging technique to study selected samples before and after annealing. Calcined specimens were measured as a powder due to partial brittle failure. In agreement with the PXRD data (Fig. S10), the WAXS patterns confirm an amorphous precipitate before calcination (B) and revealed pronounced Debye Scherrer rings indicating the formation of spinel-type Co_3O_4 after the thermal treatment (D).

The SAXS data of the composite spirals (A) can be interpreted by analyzing prominent scaling laws. This concept implies that the definition of one particle does not necessarily encompass the entire object, but

can also refer to a real domain within the particle. In that respect, meso- and nano-scaled materials are described in terms of their (sub-) dimensions, i.e. 1D-, 2D- or 3D-objects in case of needles, sheets, or spheres, respectively. The corresponding scattering contribution I(q) characteristically scales with q^{-1} (1D), q^{-2} (2D), and q^{-4} (3D).

The SAXS intensity of the here investigated polymer/mineral micro-scroll (A, violet) exhibits a q^{-2} scaling law (grey dashed line) for $q < 0.1$ nm^{-1}, as expected based on the 2D-morphology of the coiled film fragments. At intermediate values of q (0.1 nm$^{-1} < q < 0.8$ nm^{-1}), a broad shoulder is observed, proving the existence of an internal nanostructure, which presumably originates from entrapped PEI domains or pores, possibly hosting additional water, within the amorphous basic cobalt carbonate phase. The pronounced shoulder-like scattering contribution is well described by a model of polydisperse circular cylinders exhibiting a radius of R = 3.5 ± 0.7 nm and a length of L = 70 ±10.5 nm. Thus, the data are in agreement with a granular substructure of the spirals due to randomly orientated rod-like pores or occlusions of PEI.

Local variations in the PEI content and the nanostructural motifs within the composite are discussed as a possible driving force for curling. In view of the scattering signature, the formation of a gradient with respect to the material density (e.g due to polymer occlusion) along the surface normal of the 2D mineral sheets, would result in a diffuse interface reflected in a change of the power-law. Specifically, in the regime of large values of q ($q > 0.8$ nm^{-1}) a scaling law exponent of q^{-4} corresponds to a sharp interface or homogeneous structure (Porod's law), whereas a lower scaling exponent of q^{-2} as observed in our system before annealing (A), points to a diffuse interface or heterogeneous structure.[10] Removal of PEI by calcination, however, increases the scattering contrast, but is accompanied by a transformation of amorphous $Co(OH)_x(CO_3)_y$ into crystalline Co_3O_4. The reorganization of the nanostructure during the annealing treatment results in Porod-like behavior ($I(q) \sim q^{-4}$), thus indicating the formation of crystallites delineated by sharp interfaces. The characteristic q^{-1} power law behavior at low q is interpreted as the contribution of the nanopores (1D) within the calcined material. The cross-over point between q^{-1} and q^{-4} points to a correlation length ξ of ca. 50 nm (approximation $2\pi/q = \xi$), which may be related to the dimension of primary Co_3O_4 nanoparticles. In literature, Co_3O_4 nanoparticles are often reported as spherical (i.e. isometric) on average due to their cubic crystal structure. Indeed, the scattering of polydisperse spheres with radius of R = 20 ± 3 nm (Gaussian distribution) describes the experimental data in a limited q range ($q < 0.1$ nm^{-1}) rather well (yellow line in C). In summary, we propose that the Co_3O_4 powder particles comprise a porous material of cemented primary particles interspersed by pores.

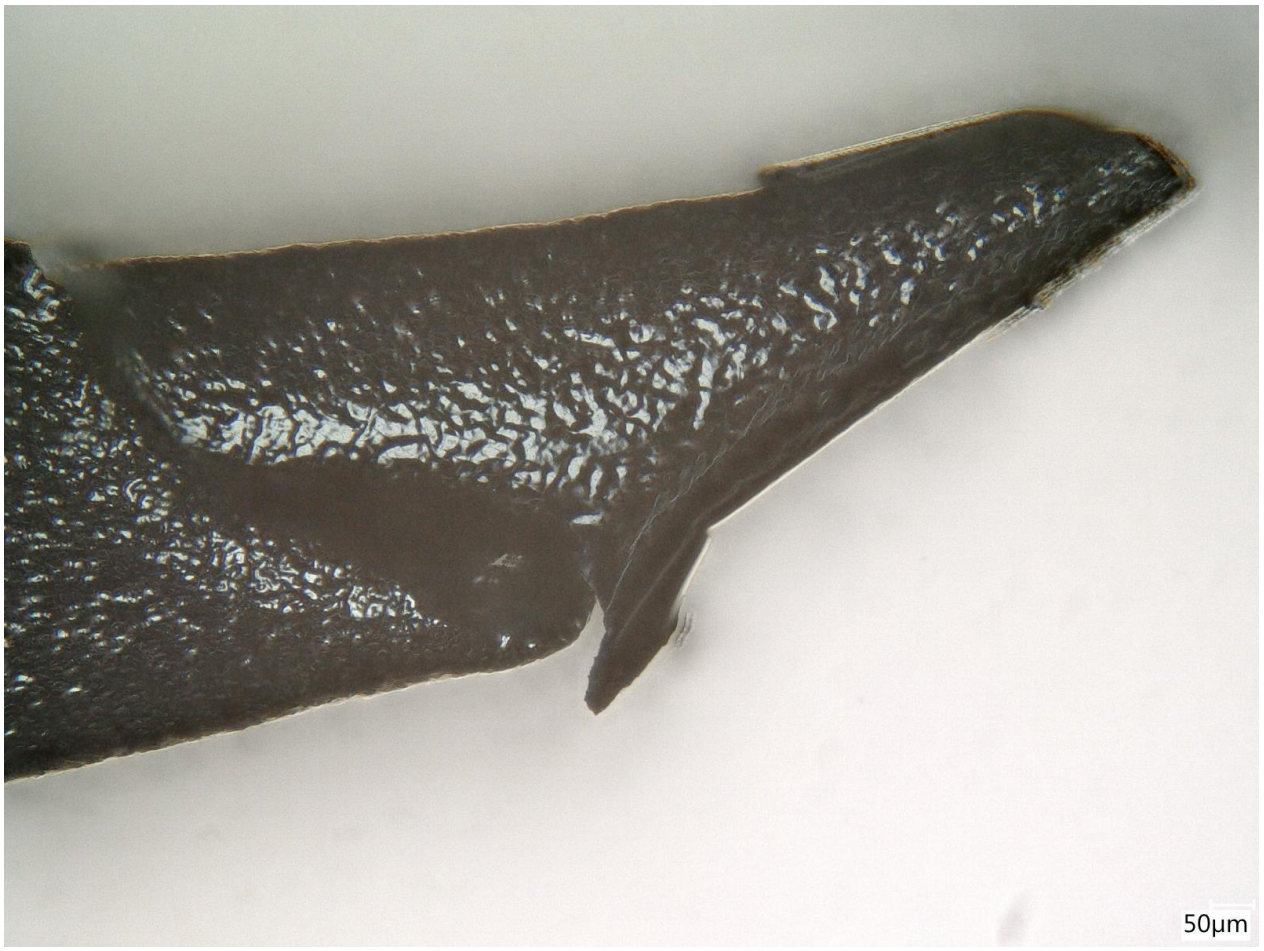

Figure S12. Light microscopy image of the calcination product obtained by annealing the curly basic cobalt carbonate precursor (deposited in the presence of [PEI] = 0.5 g/L) at 400 °C for 24 h. The general spiral morphology is intact, thus demonstrating the connectivity of the structure. The black colour is characteristic of cobalt(II,III) oxide.

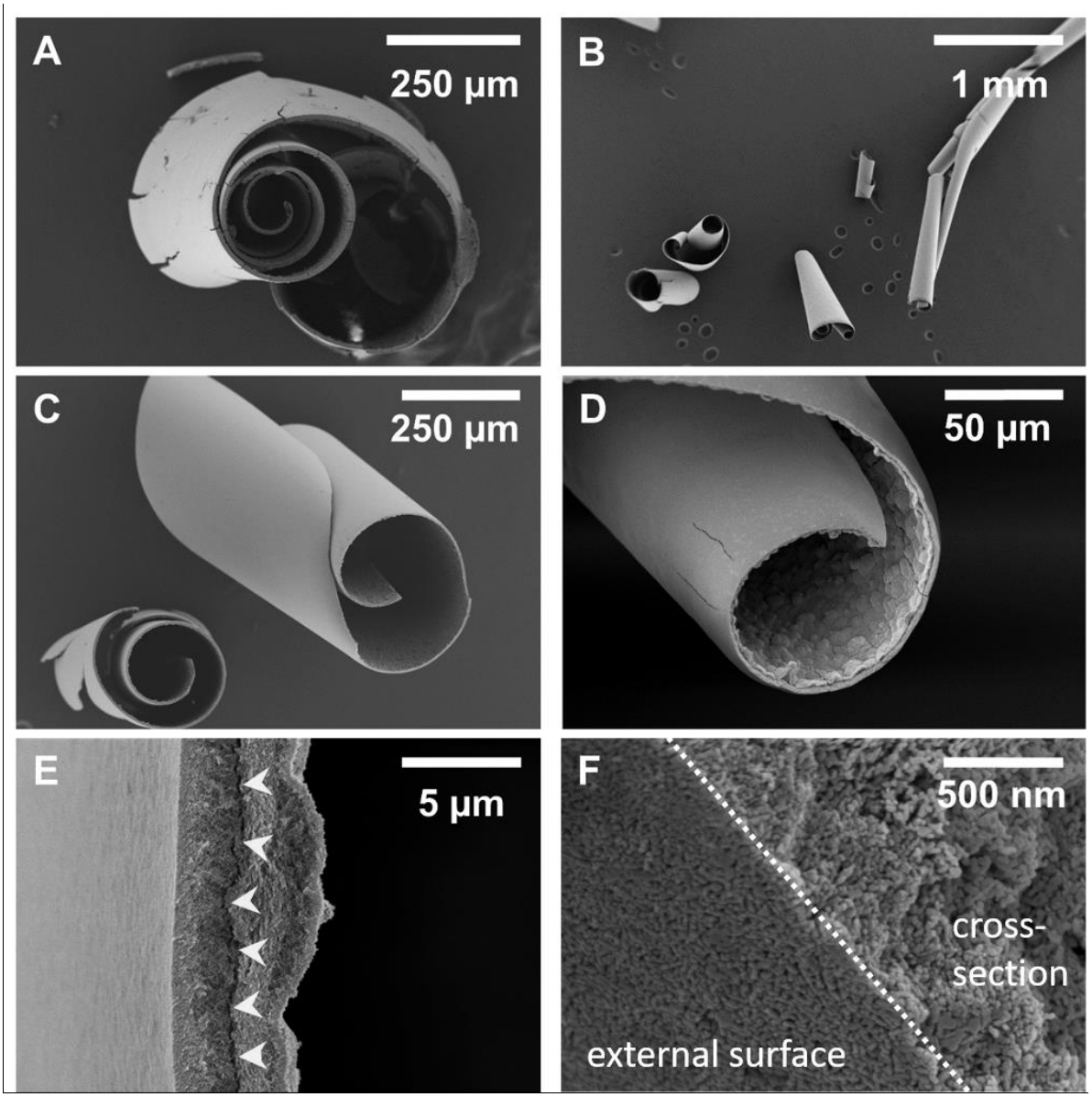

Figure S13. Scanning electron micrographs obtained from curly basic cobalt carbonate deposited at the air/solution interface in the presence of [PEI] = 0.5 g/L subjected to calcination at 400 °C for 24 h, which induces a pseudomorphic transformation to Co_3O_4. The spiral morphology is largely preserved despite volume shrinkage due to the release of CO_2 and H_2O during the decomposition of the basic cobalt carbonate precursor (A). Upon calcination, a significant fraction of the spirals (ca. 75% based on visual inspection of the precipitate) retains their structural integrity and connectivity over macroscopic dimensions despite becoming more fragile and prone to crack formation (B, overview). Reduction of the heating rate to 2K/min substantially reduces the occurrence of visible micro-cracks, thus highlighting the importance of a gentle annealing protocol (C). While vertical micro-cracks with a length of 10-100 µm are occasionally seen on the outer surface of the spirals (D), lateral delamination along the layers of the

mineral film is much more prominent (E, arrow heads pointing towards the separation line between two distinct domains). At the nanoscale, the structure is composed of interconnected nanocrystals interspersed by pores throughout the film (F).

3. References

1. H. B. Xing, H. M. Pan, Y. Fang, X. Y. Zhou, Q. Pan and D. Li, *Oncology letters*, 2014, **7**, 487-492.
2. B. G. Frushour and J. L. Koenig, *Biopolymers*, 1974, **13**, 1809-1819.
3. J. Yang, H. Cheng and R. L. Frost, *Spectrochimica Acta Part A: Molecular and Biomolecular Spectroscopy*, 2011, **78**, 420-428.
4. H. G. Brittain, *Profiles of Drug Substances, Excipients and Related Methodology*, Elsevier Science, 2011.
5. A. S. Schenk, S. Eiben, M. Goll, L. Reith, A. N. Kulak, F. C. Meldrum, H. Jeske, C. Wege and S. Ludwigs, *Nanoscale*, 2017, **9**, 6334-6345.
6. T. Wen, F. Qu, N. B. Li and H. Q. Luo, *Arabian Journal of Chemistry*, 2017, **10**, S1680-S1685.
7. R. S. Kumar, S. Arunachalam, V. S. Periasamy, C. P. Preethy, A. Riyasdeen and M. A. Akbarsha, *Polyhedron*, 2008, **27**, 1111-1120.
8. F. Román, P. Colomer, Y. Calventus and J. M. Hutchinson, *Materials*, 2018, **11**, 410.
9. X. Liu and C. T. Prewitt, *Physics and Chemistry of Minerals*, 1990, **17**, 168-172.
10. H. D. Bale and P. W. Schmidt, *Physical Review Letters*, 1984, **53**, 596-599.